 CMES, vol.14, no.3, pp.141-152, 2006

Meshless Local Petrov-Galerkin (MLPG) Mixed Collocation Method For Elasticity Problems

S. N. Atluri[1], H. T. Liu[2], and Z. D. Han[2]

Abstract: The Meshless Local Petrov-Galerkin (MLPG) mixed collocation method is proposed in this paper, for solving elasticity problems. In the present MLPG approach, the mixed scheme is applied to interpolate the displacements and stresses independently, as in the MLPG finite volume method. To improve the efficiency, the local weak form is established at the nodal points, for the stresses, by using the collocation method. The traction boundary conditions are also imposed into the stress equations directly. It becomes very simple and straightforward to impose various boundary conditions, especially for the high-order PDEs. Numerical examples show that the proposed MLPG mixed collocation method possesses a stable convergence rate, and is more efficient than the other MLPG implementations, including the MLPG finite volume method.

keyword: MLPG, Meshless, Mixed method, Collocation

1 Introduction

The meshless methods have inherent advantages over the element-based approaches, due to the elimination of the mesh and the high-order continuity of the trial functions. Therefore, the meshless methods have become an important tool in computational solid mechanics, especially for solving the problems with severe distortion, discontinuities, and moving boundaries. Tremendous efforts have been made in the research and practice of the meshless approaches, such as the smooth particle hydrodynamics (SPH) and the element free Galerkin method (EFG). However, these approaches require certain meshes or background cells for the purpose of the integration of the weak form and therefore are not truly meshless methods. Recently, Atluri and Zhu [Atluri and Zhu (1998); Atluri (2004)] proposed the truly Meshless Local Petrov-Galerkin (MLPG) approach, in which both the trial functions and test functions are constructed on local subdomains, and no background integration cells are required. In the MLPG framework, the choice of the trail and test functions is flexible, and thus various meshless methods can be constructed by different combinations of the trial and test functions.

Generally speaking, the meshless method is intrinsically more expensive than the traditional element-based method such as the finite element method. One source of the high expense lies in the fact that the meshless method usually involves more nodes for interpolation, and thus results in a larger bandwidth of the stiffness matrix than the finite element method. In addition, the shape functions formed in the meshless method usually have more complicated rational form, and thus require more Gaussian points for accurate integration. The complexity and high computational expense prevent the meshless method from fully fulfilling its potential. The MLPG method provides the flexibility in the choice of the test and trial functions and therefore makes it possible to simplify the meshless implementation. For example, in Atluri et al. (2004), the Heaviside function is adopted as the test function; thus the domain integration in the local weak form is avoided, and only boundary integration is required. Furthermore, the so-called "mixed" interpolation algorithm, wherein both the displacements and the displacement gradients are interpolated using the same shape functions, independently, has recently been proposed [Atluri, Han, and Rajendran (2004)]. The compatibility between the displacements and the displacement-gradients is enforced only at the nodal points. Through these efforts, the continuity requirement on the trial functions is reduced by one order and the complex second derivatives of the shape function are avoided. High-performance implementations of the MLPG mixed finite volume method (MFVM) were reported for elasto-static problems [Atluri, Han, Rajendran (2004), Han, Atluri (2004a)], elasto-dynamic problems

[1] Center for Aerospace Research & Education, University of California, Irvine

[2] Knowledge Systems Research, LLC, Forsyth, GA

[Han, Atluri (2004b)], nonlinear problems [Han, Rajendran, Atluri (2005)], and dynamic problems with large deformation and rotation [Han et al. (2006); Liu et al. (2006)].

The collocation method is attractive, because of its ease of implementation and efficiency. Compared with the finite volume method, the traditional collocation method suffers from the instability due to the ill-conditioned system equations formed by enforcing the balance of momentum and traction boundary conditions at nodes. Onate et al. [Onate et al. (2001)] proposed a stabilization technique by introducing new terms in both the governing equations and the traction boundary conditions. However, these artificial terms serve only for the stabilization purposes, and are only suitable for some special problems.

In the present paper, we propose a MLPG mixed collocation method and hope to further improve the computational efficiency and ease of the meshless implementation. In the present MLPG collocation approach, the moving least squares (MLS) is adopted to construct the trial functions from discrete nodes directly, and thus no mesh or the nodal connectivity is required. The "mixed" interpolation is adopted in the present method, namely, both the displacements and stresses are interpolated using the same shape functions independently, and the compatibility condition is enforced only at the nodal positions. The system equations are established at the nodes through the collocation method. Both the natural and essential boundary conditions are applied directly in the system equations, which are established in stress and displacement space from the mixed interpolation. Several numerical examples are presented, including the patch test, a cantilever beam under a transverse load, a curved beam under a transverse load, and a infinite plate with a circular hole under an uniaxial load. The computational results are compared with the theoretical predictions to demonstrate the accuracy of the MLPG mixed collocation method. Compared with the MLPG Finite Volume Method (MFVM), the proposed MLPG collocation method is not only easier to implement but also achieves more efficiency. In the present study, only elasto-static problems are presented. It is expected that the general MLPG collocation framework will be implemented in a variety of problems including large deformations and dynamics, in the very near future.

2 Meshless Interpolation

Among the available meshless approximation schemes, the moving least squares (MLS) is generally considered to be one of the best methods to interpolate random data with a reasonable accuracy, because of its completeness, robustness and continuity. The MLS is adopted in the current MLPG collocation formulation, while the implementation of other meshless interpolation schemes is straightforward within the present framework. For completeness, the MLS formulation is briefly reviewed here, while more detailed discussions on the MLS can be found in Atluri (2004).

With the MLS interpolation, a function $u(\mathbf{x})$ can be approximated over a number of scattered local points (nodes) $\{\mathbf{x}_I\}$, $(I = 1,2,...,m)$ as

$$u(\mathbf{x}) = \mathbf{p}^T(\mathbf{x})\mathbf{a}(\mathbf{x}) \tag{1}$$

where $\mathbf{p}^T(\mathbf{x})$ is a monomial basis, and $\mathbf{a}(\mathbf{x})$ is a undetermined coefficient vector. The linear monomial basis can be expressed as $\mathbf{p}^T(\mathbf{x}) = [1, x_1, x_2]$ for two-dimensional problems and $\mathbf{p}^T(\mathbf{x}) = [1, x_1, x_2, x_3]$ for three dimensional problems, respectively. The coefficient vector $\mathbf{a}(\mathbf{x})$ is determined by minimizing the weighted discrete L_2 norm, defined as

$$J(\mathbf{x}) = \sum_{I=1}^{m} w_I(\mathbf{x})[\mathbf{p}^T(\mathbf{x}_I)\mathbf{a}(\mathbf{x}) - \widetilde{u}^I]^2 \tag{2}$$

where $w_I(\mathbf{x})$ are the weight functions and $\widetilde{u}^I$ are the fictitious nodal values. Once the coefficient vector $\mathbf{a}(\mathbf{x})$ is determined and substituted into Eq. (1), the function $u(\mathbf{x})$ can be approximated by these nodal values as

$$u(\mathbf{x}) = \sum_{I=1}^{m} \Psi^I(\mathbf{x})\hat{u}^I \tag{3}$$

where $\hat{u}^I$ is the virtual nodal value at node I, and $\Psi^I(\mathbf{x})$ is the shape function. The detailed derivations and formulations can be found in Atluri (2004).

It should be noted that generally speaking, the MLS shape function does not have the Dirac Delta property, namely

$$u^I \equiv u(\mathbf{x}^I) = \sum_{J=1}^{m} \Psi^J(\mathbf{x}^I)\widetilde{u}^J \neq \widetilde{u}^I \tag{4}$$

However, with the mapping relationship between the virtual and true nodal values [Eq. (4)], it is straightforward to establish the trial functions in the true nodal values space as

$$u(\mathbf{x}) = \sum_{I=1}^{m} \Phi^I(\mathbf{x}) u^I \tag{5}$$

The detailed formulations and discussions for the MLS interpolation on the true nodal values can be found in Atluri (2004). It is worthy to mention that the weight function $w_I(\mathbf{x})$ defines the range of the influence of node I. Normally it has the radial form with a compact support size. A fourth order spline weight function is used in the present study. The node whose influence region covers the point $\mathbf{x}$ is called the neighbor node of $\mathbf{x}$. To obtain non-singular shape functions, there are at least m linearly independent neighbor nodes for the point $\mathbf{x}$. Here m is related with the order of the monomial basis t as

$$m = \begin{cases} (t+1)(t+2)/2 & \text{for 2D} \\ (t+1)(t+2)(t+3)/6 & \text{for 3D} \end{cases} \tag{6}$$

3 MLPG Mixed Collocation Method

In this section, we propose the MLPG collocation method to solve linear elastic solid mechanics problems.

3.1 Linear Elasticity

For a linear elastic body Ω undergoing infinitesimal deformations, the equations of balance of linear momentum can be written as

$$\sigma_{ij,j} + f_i = 0 \tag{7}$$

with the boundary conditions

$$\begin{aligned} &u_i = \overline{u}_i \text{ on } \Gamma_u \\ &t_i = \sigma_{ij} n_j = \overline{t}_i \text{ on } \Gamma_t \end{aligned} \tag{8}$$

In the above equations, f_i is the body force; $\overline{u}_i$ and $\overline{t}_i$ are the prescribed displacements and tractions on the displacement boundary Γ_u and traction boundary Γ_t, respectively. n_j is the outward unit normal to the boundary Γ. In the present study, the isotropic linear elastic constitutive relation is assumed, namely the stress tensor σ_{ij} is linearly related to the strain tensor ε_{ij} as

$$\sigma_{ij} = C_{ijkl} \varepsilon_{kl} \tag{9}$$

with C_{ijkl} is the elasticity tensor that has the following format for isotropic materials

$$C_{ijkl} = \lambda \delta_{ij} \delta_{kl} + \mu \left(\delta_{ik} \delta_{jl} + \delta_{il} \delta_{jk} \right) \tag{10}$$

with λ and μ are the Lame's constants. For infinitesimal deformations, the strain tensor is related to the displacement u_i as

$$\varepsilon_{ij} = \frac{1}{2} \left(u_{i,j} + u_{j,i} \right) \tag{11}$$

3.2 MLPG Mixed Collocation Method

Within the general MLPG framework, one may choose the Dirac Delta function as the test function for the unsymmetric local weak form, and apply it to each nodal point. The momentum balance equation is enforced at nodal points, as

$$\sigma_{ij,j}(\mathbf{x}^I) + f_i^(\mathbf{x}^I) = 0; \quad \text{for } I = 1, 2, ..., N \tag{12}$$

where N is the number of total nodes in the solution domain.

In the present mixed scheme, we interpolate the displacements $u_i(\mathbf{x})$ and the stresses $\sigma_{ij}(\mathbf{x})$ independently using the same shape functions obtained from the MLS approximation [Eq. (3)], namely

$$u_i(\mathbf{x}) = \sum_{J=1}^{m} \Phi^J(\mathbf{x}) u_i^J \tag{13}$$

$$\sigma_{ij}(\mathbf{x}) = \sum_{J=1}^{m} \Phi^J(\mathbf{x}) \sigma_{ij}^J \tag{14}$$

Here, u_i^J and σ_{ij}^J are the nodal displacements and stresses at node J, respectively. Upon substituting the stress interpolation Eq. (14) into Eq. (12), we have

$$\sum_{J=1}^{m} \Phi_{,j}^J(\mathbf{x}^I) \sigma_{ij}^J + f_i(\mathbf{x}^I) = 0; \quad \text{for } I = 1, 2, ..., N \tag{15}$$

It is clearly shows that there are no second derivatives of the shape functions involved in the system equations due to the independent interpolation of stress variables. It is well known that the meshless approximation, specifically the MLS, usually has very complex form of the second

derivatives. Therefore, by adopting the mixed interpolation scheme, the time-consuming calculation of the second derivatives of the MLS shape functions is avoided, and the efficiency is improved. Secondly, the requirement of the continuity of the shape functions is reduced by one-order and thus a smaller nodal influence size can be chosen to speed up the calculation of the shape functions. We will show in the following numerical examples that the first order polynomials basis is usually adequate for the elasticity problems. Finally, the adoption of the stress variables in establishing the system equations provides a way to apply the traction boundary conditions directly in the system equations. We will make a detailed discussion on the application of boundary conditions in the following session.

From the Eq. (15), the number of equations is less than the number of the independent stress variables, because the nodal stress variables are more than the displacement ones. Therefore, we need to establish some more equations in addition to Eq. (15) through the stress-displacement relation [Eq. (9) and (11)]. The standard collocation method may be applied to enforce the stress-displacement relation at each nodal point. For linear elasticity problems, this relation can be written as

$$\sigma_{ij}(\mathbf{x}^I) = \frac{1}{2} C_{ijkl} \left[u_{k,l}(\mathbf{x}^I) + u_{l,k}(\mathbf{x}^I) \right] \tag{16}$$

and with the interpolations of the displacements [Eq. (13)] and stresses [Eq. (14)], we have

$$\sigma_{ij}^I = \frac{1}{2} C_{ijkl} \sum_{J=1}^{m} \left[\Phi_{,l}^J(\mathbf{x}^I) u_k^J + \Phi_{,k}^J(\mathbf{x}^I) u_l^J \right] \tag{17}$$

Finally, we can rewrite the system equations of Eq. (15) and (17) as

$$\mathbf{K}_s \cdot \mathbf{S} = \mathbf{f}_b \tag{18a}$$

$$\mathbf{S} = \mathbf{T} \cdot \mathbf{u} \tag{18b}$$

Here, $\mathbf{f}_b$ is the body force vector; $\mathbf{S}$ and $\mathbf{u}$ are the nodal stress component vector and the nodal displacement component vector, respectively. The number of the equations is equal to the number of the total degrees of freedom (nodal displacements and stresses). Therefore, it is solvable with properly proposed boundary conditions.

3.3 Boundary Conditions

The traction boundary conditions are enforced at each of the traction boundary nodes K, as:

$$\sigma_{ij}^K n_j^K = \bar{t}_i^K; \quad \text{for } K = 1, 2, ..., N_s \tag{19}$$

with N_s is the number of the traction boundary nodes, and $\mathbf{n}^K$ is the outward normal at the boundary node K. Eq. (19) can be rewritten in term of the stress component vector, as

$$\mathbf{M}^K \cdot \mathbf{S}^K = \bar{\mathbf{t}}^K; \quad \text{for } K = 1, 2, ..., N_s \tag{20}$$

where $\mathbf{M}^K$ is the general coupling matrix between the stress components, representing the traction boundary conditions.

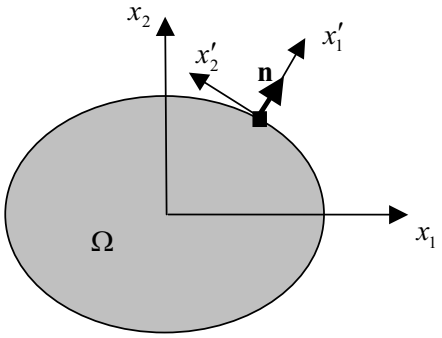

Figure 1 : The local coordinates system

If the normal $\mathbf{n}^K$ is parallel to the global coordinates, $\mathbf{M}^K$ is a diagonal unit matrix. For the nodes with the normal not being parallel to the global coordinates, a local coordinate system can be defined, by taking the local $\mathbf{x}'^K_1$ direction coinciding with the outward normal direction $\mathbf{n}^K$, as shown in Fig. 1. Eq. (20) can be rewritten in the local coordinate system,

$$\mathbf{M}'^K \cdot \mathbf{S}'^K = \bar{\mathbf{t}}^K; \quad \text{for } K = 1, 2, ..., N_s \tag{21}$$

where
$\mathbf{S}'^K = \mathbf{Q}^K \cdot \mathbf{S}^K$; $\mathbf{M}'^K = \mathbf{M}^K \cdot (\mathbf{Q}^K)^{-1}$and $\mathbf{Q}^K$ the local transformation matrix between the coordinates. With the use of the local coordinate system, we can represent the known stress degrees of freedom (DOFs) as $\mathbf{S}'_1 = \bar{\mathbf{t}}$ and the other unknown stress DOFs as $\mathbf{S}_2$. Eqs. 3.3 and (21) can be written for the system equations as,

$$\mathbf{K}_{1_s} \cdot \mathbf{Q}^{-1} \cdot \mathbf{S}'_1 + \mathbf{K}_{2_s} \cdot \mathbf{S}_2 = \mathbf{f}_b \tag{22a}$$

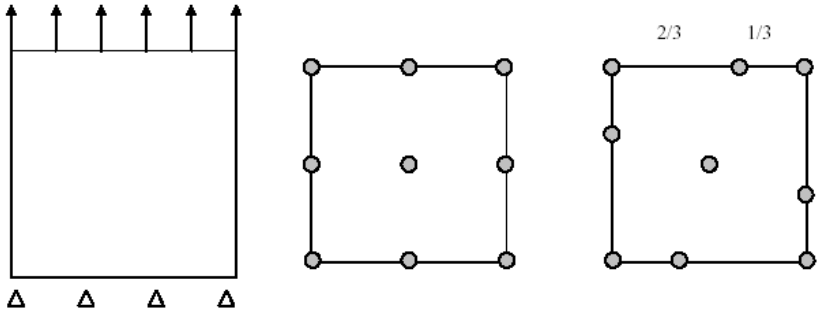

Figure 2 : The patch test: a rectangle under uniform tension. The two nodal configurations

$$\mathbf{S}'_1 = \mathbf{Q}\cdot\mathbf{T}_1\cdot\mathbf{u} \equiv \mathbf{T}'_1\cdot\mathbf{u} \tag{22b}$$

$$\mathbf{S}_2 = \mathbf{T}_2\cdot\mathbf{u} \tag{22c}$$

and

$$\mathbf{S}'_1 = \bar{\mathbf{t}} \tag{23}$$

Thereafter the traction boundary conditions in Eq. (23) can be enforced by imposing it into Eq. (22)b, by using the penalty method, as

$$(1+\alpha)\mathbf{S}'_1 = \mathbf{T}'_1\cdot\mathbf{u} + \alpha\bar{\mathbf{t}} \tag{24}$$

or

$$\mathbf{S}'_1 = \frac{1}{(1+\alpha)}\mathbf{T}'_1\cdot\mathbf{u} + \frac{\alpha}{(1+\alpha)}\bar{\mathbf{t}} \tag{25}$$

where α is the penalty number which is set to be 10^6 in the present study. By substituting Eq. (25) into Eq. (22)a, the system equations are expressed in term of the displacement DOFs,

$$\mathbf{K}\cdot\mathbf{u} = \mathbf{f} \tag{26}$$

where

$$\begin{aligned}\mathbf{K} &= \mathbf{K}_{1_s}\cdot\mathbf{Q}^{-1}\cdot\left[\frac{1}{(1+\alpha)}\mathbf{T}'_1\right] + \mathbf{K}_{2_s}\cdot\mathbf{T}_2 \\ \mathbf{f} &= \mathbf{f}_b - \mathbf{K}_{1_s}\cdot\mathbf{Q}^{-1}\cdot\left[\frac{\alpha}{(1+\alpha)}\bar{\mathbf{t}}\right]\end{aligned} \tag{27}$$

It should be noted that the transformation of the system equations is only related to the stress components related to the traction boundary node, and is done locally. The transformation matrix $\mathbf{Q}$ is not formed explicitly. Therefore, this transformation process is numerically efficient. By imposing the displacement boundary conditions into Eq. 4, the system equations can be solved with the displacement DOFs [Han and Atluri (2004a)].

4 Numerical Examples

In this section, several 2D numerical examples, which are solved by the proposed MLPG mixed collocation method, are presented. The examples include: 1) the patch test, 2) a cantilever beam under a transverse load, 3) a curved beam bent by a force at the end, and 4) an infinite plate with a circular hole under uniaxial load.

4.1 The Patch Test

The standard patch test: a rectangle under uniform tension load (see Fig. 2) is solved as the first example. The material parameters are as follows: the Young's modulus $E = 1.0$, and the Poisson's ratio $v = 0.25$. Plane stress condition is assumed for the 2D problem and 9 nodes are used. Two nodal configurations are used for the testing: one is regular, and another is irregular, as shown in Fig. 2. The proper displacement constraints are applied to the bottom edge.

The simulation results show a linear displacement on the lateral edges, and constant displacement on the top edge; the normal stress in the loading direction is constant and there is no shear stress in the solution domain.

4.2 Cantilever Beam

In the second example, we solve a cantilever beam under a transverse load at the end, as shown in Fig. 3. For this problem, the exact displacement solution for plane stress

Figure 3 : A cantilever beam under a transverse load at the end

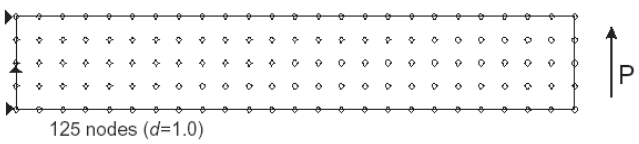

Figure 4 : The nodal configuration of the cantilever beam for d=1.0

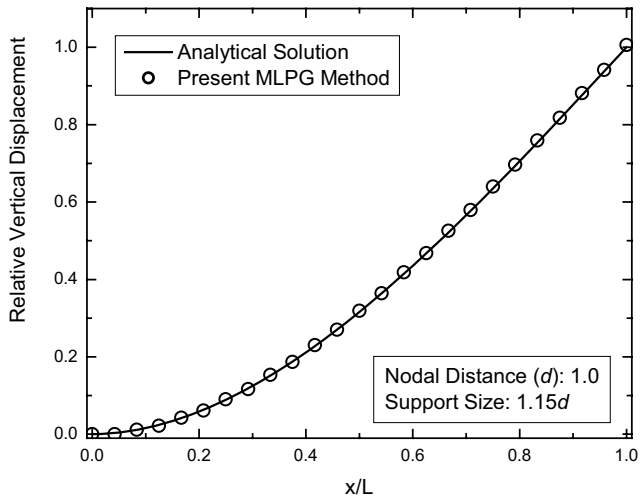

Figure 5 : The normalized vertical displacement of the cantilever beam under the end load

is given in Timoshenko and Goodier (1970) as

$$u_x = -\frac{Py}{6EI}\left[3x(2L-x)+(2+v)\left(y^2-c^2\right)\right]$$
$$u_y = \frac{Py}{6EI}\left[x^2(3L-x)+3v(L-x)y^2+(4+5v)c^2x\right] \tag{28}$$

where the moment of inertia $I = c^3/3$.

The problem is solved using the MLPG collocation method under plane stress condition with the following constants: $P = 1$, $E = 1$, $c = 2$, $L = 24$, and $v = 0.25$. Regular uniform nodal configurations with nodal distances, d, of 1.0, 0.5, and 0.25 are used. The corresponding numbers of nodes are 125, 441, and 1649, respectively. The nodal configuration for $d = 1.0$ is shown in Fig. 4.

This problem is simulated using the MLS with the first order polynomial basis. The support size is chosen as $1.15d$. Fig. 5 shows the normalized vertical displacement along the central line of the beam for the nodal configuration with $d = 1.0$. The simulation prediction agrees with the analytical solution very well. The relative error of the maximum vertical displacement is less than 0.6% for this relatively coarse nodal configuration (125 nodes).

The support size (the size of the influence domain) is a very important parameter in meshless methods. It is related to both the accuracy of the solution, as well as the computational efficiency. On one hand, a too smaller support size will cause the meshless approximation algorithms singular, since enough neighbor nodes are not included. On the other hand, a too large support size leads to the loss of the interpolation locality. In the current study, circular support domains are adopted for the 2D problems, with the radius being defined as the support size. Four support sizes are chosen for the cantilever beam problem and they are defined to be proportional to the nodal distance as 1.15, 1.3, 1.5, and 1.8. Two nodal configurations are used (d =1.0 and 0.5) for the current simulations. Fig. 6 shows that accurate results are obtained for small support sizes and the results are also less sensitive to the support size when it is small. This observation is encouraging since small support size makes the present method even more efficient by speeding up the MLS approximation and reducing the bandwidth of the stiffness matrix.

The convergence rate is studied with three nodal configu-

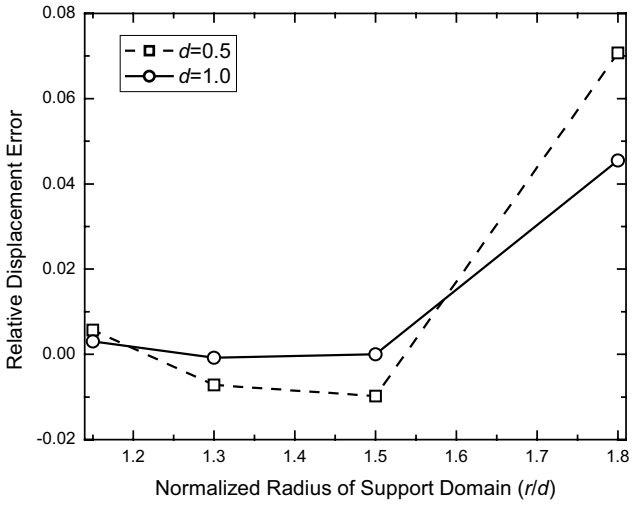

Figure 6 : The influence of the support size in the cantilever beam under the end load

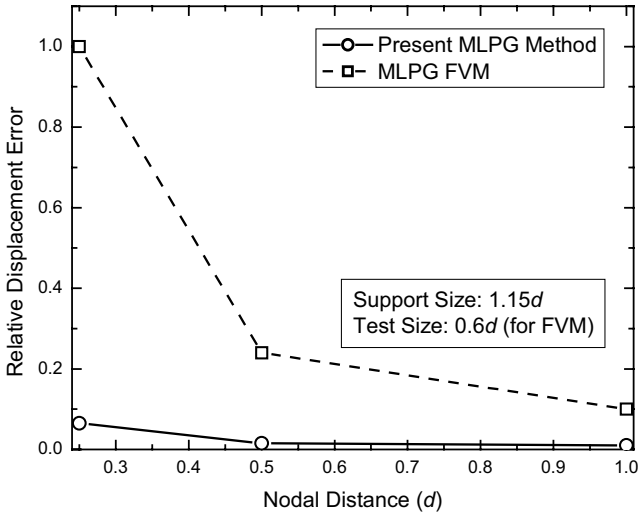

Figure 8 : CPU Time comparison between MLPG/Mixed finite volume method and MLPG/Mixed collocation method

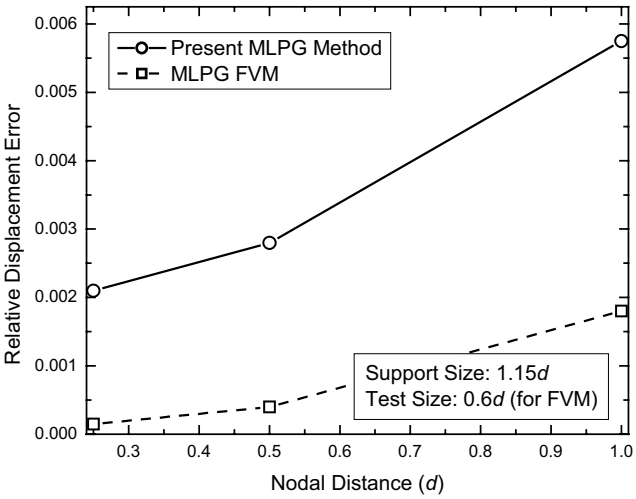

Figure 7 : The convergence rate in the cantilever beam under the end load

rations (d =1.0, 0.5, and 0.25) and the support size 1.15d. The maximum relative errors of the vertical displacement are used for showing the convergence rate in Fig. 7. The results clearly show that a stable convergence is obtained for the present MLPG method. The relative error is less than 0.6% for the coarse nodes (d =1.0) and about 0.2% for the fine nodal configuration (d =0.25). The convergence rate of the same problem using the MLPG Finite Volume Method (MLPG FVM) [Atluri, Han, Rajendran (2004)] is also shown in this figure. The test size in the MLPG FVM simulations is set to 0.6d as suggested by the authors, for the best results. As expected, more accurate results are obtained using the MLPG FVM than the current MLPG collocation method. However, the increase in the accuracy of MLPG FVM is achieved with an increase in the computational expense. In the FVM, a boundary integration of the local weak form is required, and a special numerical quadrature technique and many Gaussian points are critical for the accurate calculation of the boundary integration involving complex forms of shape functions. Fig. 8 compares the CPU time requirement of the current MLPG method, with the MLPG FVM. The CPU time shown in Fig. 8 is normalized so that the maximum value in this figure is 1. From the comparison, it is clearly seen that the present MLPG collocation method is much more efficient than the MLPG FVM. The CPU times of the FVM are over 10 times larger than the corresponding times of the present MLPG collocation method. In computational mechanics, there is always a compromise between accuracy and efficiency. The proposed MLPG mixed collocation method achieves a reasonable accuracy with stable convergence rate, with much less computational expense. It should be mentioned that the MLPG FVM used here for comparison purposes, is recognized as a very efficient meshless implementation, and it even out-performs the finite element method for some problems [Han, Atluri (2004b)].

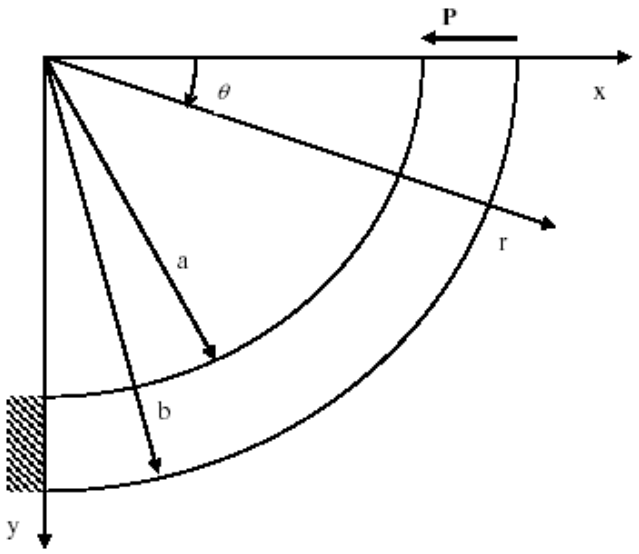

Figure 9 : A curved beam under an end load

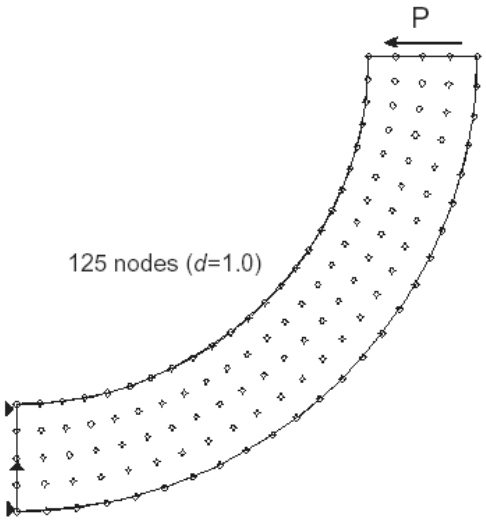

Figure 10 : The nodal configuration of the curved beam for d=1.0

4.3 Curved Beam

In this example, a curved beam under an end load is used to evaluate the present method. The problem is shown in Fig. 9, for which the following exact displacement solution for plane stress is given in Timoshenko and Goodier (1970):

$$
\begin{aligned}
&u_r = \\
&\frac{P}{E}\left[\begin{array}{l} \sin\theta\left(D(1-v)\log r + A(1-3v)r^2 + \frac{B(1+v)}{r^2}\right) \\ -2D\theta\cos\theta + K\sin\theta + L\cos\theta \end{array}\right] \\
&u_\theta = \\
&\frac{P}{E}\left[\begin{array}{l} -\cos\theta\left(-D(1-v)\log r + A(5+v)r^2 + \frac{B(1+v)}{r^2}\right) \\ 2D\theta\sin\theta + K\cos\theta + L\sin\theta \end{array}\right]
\end{aligned}
\tag{29}
$$

where the constants are defined as

$$
\begin{aligned}
&N = a^2 - b^2 + \left(a^2 + b^2\right)\log\frac{b}{a} \\
&A = \frac{1}{2N}\; B = -\frac{a^2 b^2}{2N} \\
&D = -\frac{a^2 + b^2}{2N}\; L = D\pi \\
&K = -\left(D(1-v)\log r_0 + A(1-3v)r_0^2 + \frac{B(1+v)}{r_0^2}\right) \\
&r_0 = \frac{a+b}{2}
\end{aligned}
\tag{30}
$$

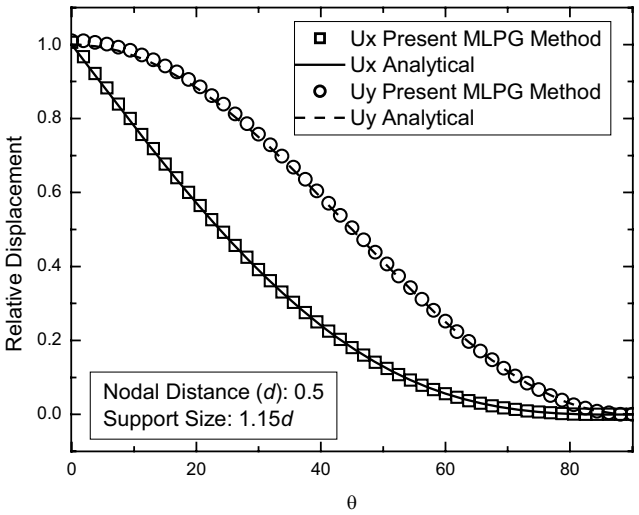

Figure 11 : The normalized vertical and horizontal displacement of the curved beam under the end load

The problem is solved for the plane stress condition, with $P = 1$, $E = 1$, $a = 13$, $b = 17$, and $v = 0.25$. Regular uniform nodal configurations with nodal distance, d, of 1.0, 0.5 and 0.25 are used. The corresponding numbers of the nodes are 125, 441, and 1649. The nodal configuration of $d = 1.0$ is shown in Fig. 10.

For the curved beam, the displacement and stress fields are more complicated than those in a straight beam, with many non-polynomial terms. However the MLS interpolation with the first order monomials basis is still used to solve this problem with a support size of $1.15d$. The

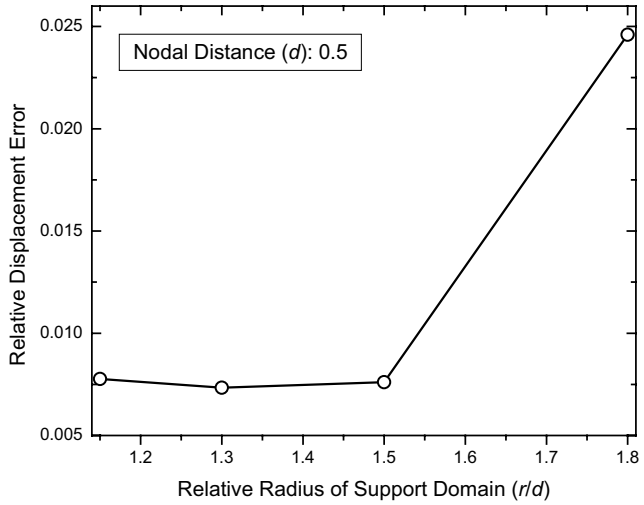

Figure 12 : The influence of the support size in the curved beam under the end load

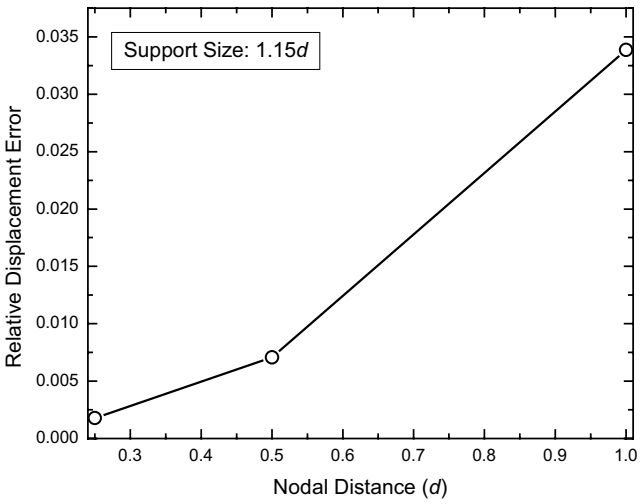

Figure 13 : The convergence rate of the curved beam under the end load

horizontal and vertical displacements for the nodal configuration with $d = 0.5$ are shown in Fig. 11 and a good agreement with the analytical solutions is obtained.

The influence of the support size is shown in Fig. 12, with the nodal distance $d = 0.5$ and support size $1.15d$. Here and in the following discussion of the curved beam problem, the relative displacement error is used to characterize the computational error. The relative displacement error is defined as

$$\varepsilon = \sqrt{\frac{1}{2}\left[\left(\frac{\vec{u}_x - u_x}{u_x}\right)^2 + \left(\frac{\vec{u}_y - u_y}{u_y}\right)^2\right]} \tag{31}$$

Here, u_x and u_y are the analytical displacement components at the center of the end of the beam, and are calculated using Eq. 4.4; while $\vec{u}_x$ and $\vec{u}_y$ are the corresponding displacement components obtained by the MLPG mixed collocation simulations. It is observed that better results are obtained for small support sizes, and the computational accuracy is not sensitive when the support size is small. This is consistent with the support size effect observed in the straight beam simulations, and again it is encouraging since small support size means less neighboring nodes and will speed up the computation. 13 shows convergence rate of the curved beam problem with three nodal configurations (d =1.0, 0.5, and 0.25), with the support size of $1.15d$. A stable and monotonic convergence rate is observed for the curved beam with less than 0.2% error for the finest nodal configuration.

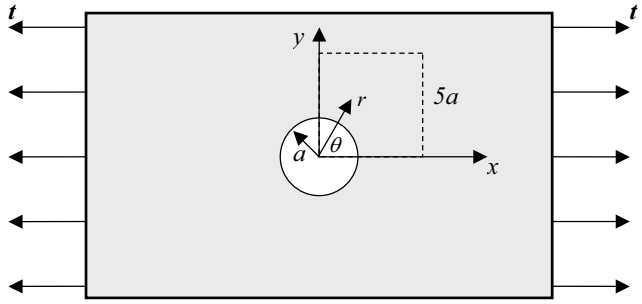

Figure 14 : An infinite plate with a circular hole under a uniaxial load

4.4 Infinite Plate with a Circular Hole

Finally, we show the computational results of an infinite plate with a circular hole subjected to a uniaxial traction P at infinity as shown in Fig. 14. The exact solutions for stresses and displacements for this problem are

$$\begin{aligned}
\sigma_x &= P\left\{1 - \frac{a^2}{r^2}\left[\frac{3}{2}\cos(2\theta) + \cos(4\theta)\right] + \frac{3a^4}{2r^4}\cos(4\theta)\right\} \\
\sigma_y &= -P\left\{\frac{a^2}{r^2}\left[\frac{1}{2}\cos(2\theta) - \cos(4\theta)\right] + \frac{3a^4}{2r^4}\cos(4\theta)\right\} \\
\sigma_{xy} &= -P\left\{\frac{a^2}{r^2}\left[\frac{1}{2}\sin(2\theta) + \sin(4\theta)\right] - \frac{3a^4}{2r^4}\sin(4\theta)\right\}
\end{aligned} \tag{32}$$

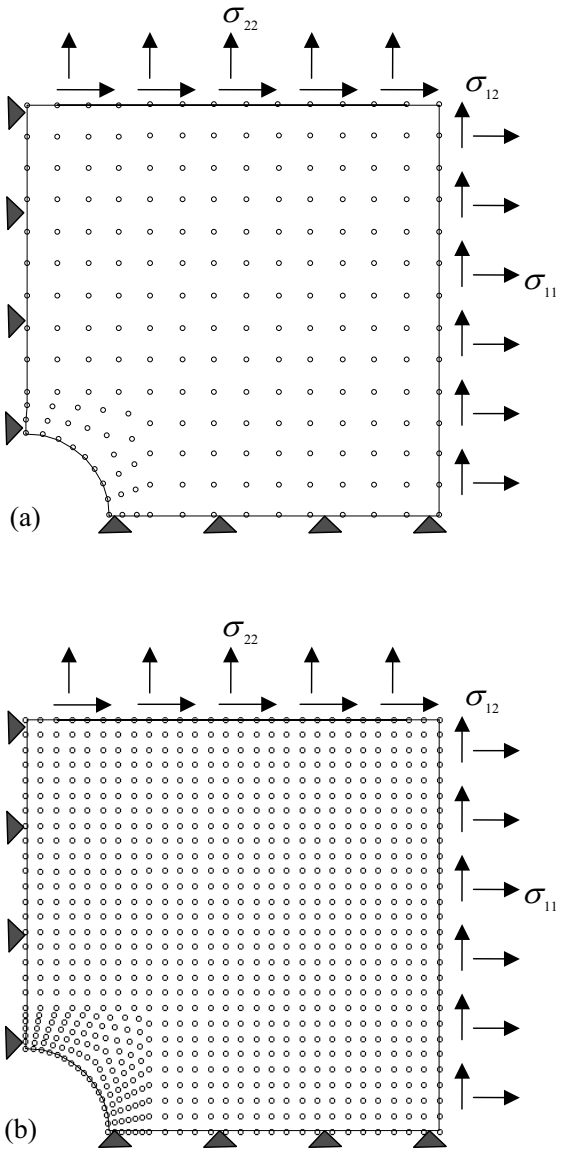

Figure 15 : : The nodal configurations and boundary conditions of the infinite plate with a circular hole (a) 389 nodes and (b) 822 nodes

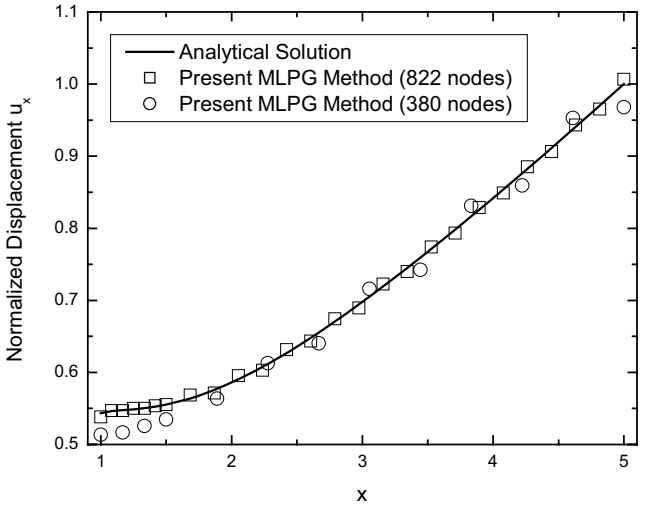

Figure 16 : The horizontal displacement along $y = 0$for the two nodal configurations

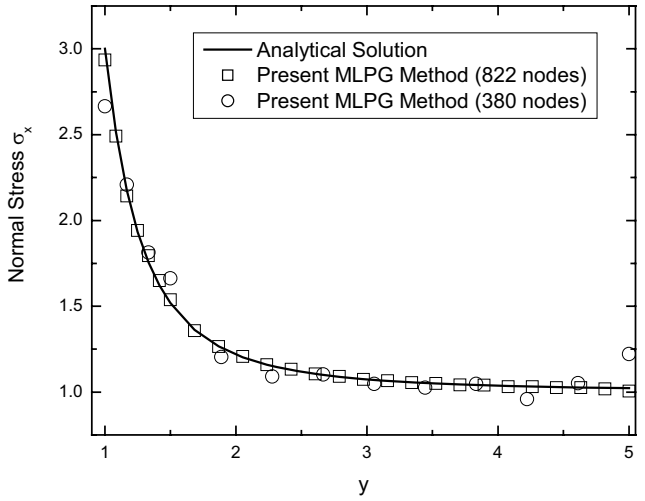

Figure 17 : The normal stress σ_x along $x = 0$ for the two nodal configurations

and

$$u_r = \frac{P}{4G}\left\{ r\left[\frac{\kappa-1}{2}+\cos(2\theta)\right] + \frac{a^2}{r}\left[1+(1+\kappa)\cos(2\theta)\right] - \frac{a^4}{r^3}\cos(2\theta)\right\}$$
$$u_\theta = \frac{P}{4G}\left\{(1-\kappa)\frac{a^2}{r} - r - \frac{a^4}{r^3}\right\}\sin(2\theta) \qquad (33)$$

respectively. In the above equations, G is the shear modulus and $\kappa = (3-\nu)/(1+\nu)$ with ν the Poisson's ratio. Due to symmetry, only the upper right square quadrant of the plate is modeled [see Fig. 14]. The edge length of the square is $5a$,with a being the radius of the circular hole. Symmetry boundary conditions are imposed on the left and bottom edges and the tractions obtained from the analytical solution [Eq. 5] are applied to the top and right edges as shown in Figure 15.

The problem is solved using the MLPG mixed collocation method, under a plane stress condition, with the following constants: $P = 1$, $E = 1$, and $\nu = 0.25$. Two nodal

configurations with 380 and 822 nodes, respectively, are used and shown in Figure 15. The MLS with linear basis is used in the simulation and the support size is $1.65d$, with d being the average nodal distance. The horizontal displacement u_x along the bottom edge $(y = 0)$, and the stress component σ_x along the left edge $(x = 0)$ are shown in Figure 16 and Figure 17, respectively. Compared with the analytical solutions, good agreements are obtained for both the displacements and stresses.

5 Closure

The MLPG mixed collocation method is developed through the MLPG framework in this paper. The mixed interpolation is adopted in the current study with the Moving Least Squares (MLS) scheme, namely the stresses and displacements are interpolated using the same shape functions independently. The collocation method is adopted for establishing the system equations. By performing a coordinate system transformation, the traction boundary conditions are converted into stress values on the boundary nodes, and therefore can be applied to the system equations directly. As a result, a very simple formulation is achieved, and the implementation is easy and straightforward. For elasticity problems, only the first derivatives of the shape functions are required, and no integration either over local domain or over the local boundary is needed. Therefore the continuity requirement on the trial functions is reduced by one-order; and the use of complex second derivatives of the shape functions are avoided. This not only improves the computational efficiency, but also results in ease of implementation. The numerical examples show that the first order monomials basis is adequate, even for the complicated curved beam problem. When the support size is kept small, more accurate and less sensitive results are obtained. The combination of first order MLS, and a small support size, requires only a few neighboring nodes, and thus will speed up the computation.

The intrinsic complexity and high computational expense are the main barriers for the meshless approaches to fully fulfill their application potentials. The MLPG mixed collocation method is presented to keep a balance between the accuracy and efficiency. Although it is demonstrated here only for static problems, in which the global system equations are required to be formed, the present method is even more efficient for solving the dynamic transient problems by using the explicit algorithms [Han, Liu, Rajendran and Atluri (2006) and Liu, Han, Rajendran and Atluri (2006)]. Since the traction boundary conditions can be imposed directly, the present MLPG mixed collocation method can be used in conjunction with iteration solvers, for better performance. The numerical examples presented in this paper demonstrate that the proposed MLPG mixed collocation method is capable of solving various solid mechanics problems efficiently with reasonable accuracy. The convergence studies in the numerical examples demonstrate that the present method is stable.

References

Atluri, S.N. (2004): The Meshless Local Petrov-Galerkin (MLPG) Method for Domain & Boundary Discretizations, Tech Science Press, 665 pages.

Atluri, S. N.; Han, Z. D.; Rajendran, A. M. (2004): A New Implementation of the Meshless Finite Volume Method, Through the MLPG "Mixed" Approach, *CMES: Computer Modeling in Engineering & Sciences*, vol. 6, no. 6, pp. 491-514.

Atluri, S. N.; Kim, H.G.; Cho, J.Y. (1999): A critical Assessment of the truly meshless local Petrov-Galerkin (MLPG) and local boundary integration equation (LBIE) methods, *Computational Mechanics*, Vol. 24, pp. 348-372.

Atluri, S. N.; Zhu, T. (1998): A new meshless local Petrov-Galerkin (MLPG) approach in computational mechanics. *Computational Mechanics*, Vol. 22, pp. 117-127.

Han, Z. D.; Atluri, S. N. (2004a): Meshless Local Petrov-Galerkin (MLPG) approaches for solving 3D Problems in elasto-statics, *CMES: Computer Modeling in Engineering & Sciences*, vol. 6 no. 2, pp. 169-188.

Han, Z. D.; Atluri, S. N. (2004b): A Meshless Local Petrov-Galerkin (MLPG) approaches for solving 3-dimensional elasto-dynamics, *CMC: Computers, Materials & Continua*, vol. 1 no. 2, pp. 129-140.

Han Z. D.; Liu H. T.; Rajendran, A. M; Atluri, S. N. (2006): The Applications of Meshless Local Petrov-Galerkin (MLPG) Approaches in High-Speed Impact, Penetration and Perforation Problems, *CMES: Computer Modeling in Engineering & Sciences*, Vol. 14, No. 2, pp. 119-128.

Liu H. T.; Han Z. D.; Rajendran, A. M; Atluri, S.

N. (2006): Computational Modeling of Impact Response with the RG Damage Model and the Meshless Local Petrov-Galerkin (MLPG) Approaches, *CMC: Computers, Materials, & Continua*, Vol. 4, No. 1, pp. 43-54.

Han, Z. D.; Rajendran, A. M; Atluri, S. N. (2005): Meshless Local Petrov-Galerkin (MLPG) Approaches for Solving Nonlinear Problems with Large Deformation and Rotation, *CMES: Computer Modeling in Engineering & Sciences*, vol. 10, no. 1, pp. 1-12.

Onate E.; Perazzo, F.; Miquel, J. (2001): A finite point method for elasticity problems, *Computers and Structures*, vol. 79, pp. 2151-2163.

Timoshenko, S.P.; Goodier, J.N. (1970): Theory of Elasticity, 3^{rd} edition, McGraw Hill.